Experimental Test of the Spin Mixing Interface Conductivity Concept

Mathias Weiler,[1,*] Matthias Althammer,[1] Michael Schreier,[1] Johannes Lotze,[1] Matthias Pernpeintner,[1] Sibylle Meyer,[1] Hans Huebl,[1] Rudolf Gross,[1,2] Akashdeep Kamra,[3] Jiang Xiao,[4] Yan-Ting Chen,[3] HuJun Jiao,[3] Gerrit E. W. Bauer,[3,5] and Sebastian T. B. Goennenwein[1,†]

[1]*Walther-Meißner-Institut, Bayerische Akademie der Wissenschaften, 85748 Garching, Germany*
[2]*Physik-Department, Technische Universität München, 85748 Garching, Germany*
[3]*Kavli Institute of Nanoscience, Delft University of Technology, 2628 CJ Delft, Netherlands*
[4]*Department of Physics and State Key Laboratory of Surface Physics, Fudan University, Shanghai 200433, China*
[5]*Institute of Materials Research and WPI-AIMR, Tohoku University, Sendai 980-8577, Japan*
(Received 20 June 2013; published 23 October 2013)

We perform a quantitative, comparative study of the spin pumping, spin Seebeck, and spin Hall magnetoresistance effects, all detected via the inverse spin Hall effect in a series of over 20 yttrium iron garnet/Pt samples. Our experimental results fully support present, exclusively spin current-based, theoretical models using a single set of plausible parameters for spin mixing conductance, spin Hall angle, and spin diffusion length. Our findings establish the purely spintronic nature of the aforementioned effects and provide a quantitative description, in particular, of the spin Seebeck effect.

DOI: 10.1103/PhysRevLett.111.176601 PACS numbers: 72.25.Mk, 72.15.Jf, 85.75.−d

Pure spin currents present a new paradigm in spintronics [1,2] and spin caloritronics [3]. In particular, spin currents are the origin of spin pumping [4,5], the spin Seebeck effect [6,7], and the spin Hall magnetoresistance (SMR) [8–10]. Taken alone, all these effects have been extensively studied, both experimentally [6–9,11–13] and theoretically [4,14–18]. From a theoretical point of view, all these effects are governed by the generation of a current of angular momentum via a nonequilibrium process. The flow of this spin current across a ferromagnet–normal-metal interface can then be detected. The relevant interface property that determines the spin current transport thereby is the spin mixing conductance. Nevertheless, there has been an ongoing debate regarding the physical origin of the measurement data acquired in spin Seebeck and SMR experiments due to possible contamination with the anomalous Nernst effect [19–21] or anisotropic magnetoresistance [22,23] caused by static proximity polarization of the normal metal [23]. Very recently, an alternative, proximity-effect based origin for the SMR has been proposed [24]. To settle this issue, a rigorous check of the consistency of the spin-current based physical models across all three effects is needed. If possible contamination effects are absent, according to the spin mixing conductance concept [25], there should exist a generalized Ohm's law between the interfacial spin current and the energy associated with the corresponding nonequilibrium process. This relation should invariably hold for the spin pumping, spin Seebeck and spin Hall magnetoresistance effects, as they are all based on the generation and detection of interfacial, nonequilibrium spin currents. We here put forward heuristic arguments that are strongly supported by experimental evidence for a scaling law that links all the aforementioned spin(calori)tronic effects on a fundamental level and allows us to trace back their origin to pure spin currents.

We carried out a systematic set of spin pumping, spin Seebeck and SMR experiments on $Y_3Fe_5O_{12}$ (YIG)/Pt thin film bilayers. In our spin pumping experiments [schematically depicted in Fig. 1(a)], we place YIG/Pt bilayers in a microwave cavity operated at $\nu = 9.85$ GHz to resonantly excite magnetization dynamics. The emission of a spin current density $\boldsymbol{J}_s$ across the bilayer interface into the Pt provides a damping channel for the nonequilibrium excitations of the magnetization $\boldsymbol{M}$. It has been

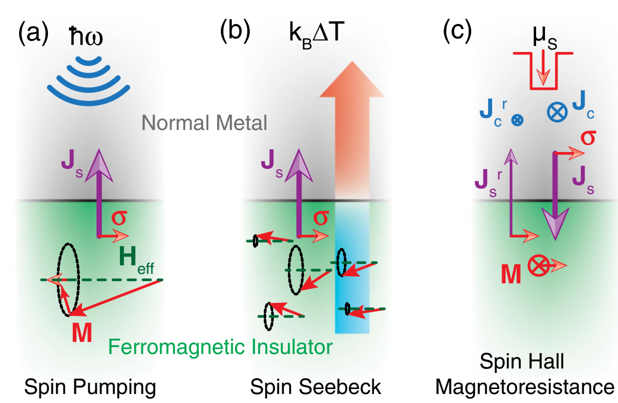

FIG. 1 (color online). (a),(b) Schematic depictions of the spin pumping and spin Seebeck effects. The magnetization $\boldsymbol{M}$ in the ferromagnet (YIG in our experiments) is excited either resonantly (a) or thermally (b). The $\boldsymbol{M}$ precession around $\boldsymbol{H}_{\mathrm{eff}}$ (see text) is damped via the emission of a spin current $\boldsymbol{J}_s$ with polarization $\boldsymbol{\sigma}$ into the normal metal (Pt in our experiments). (c) The spin Hall magnetoresistance is due to the torque exerted on $\boldsymbol{M}$ by an appropriately polarized $\boldsymbol{J}_s$ which yields a change in the reflected spin current $\boldsymbol{J}_s^r$. The interconversion between $\boldsymbol{J}_s$ ($\boldsymbol{J}_s^r$) and the charge currents $\boldsymbol{J}_c$ ($\boldsymbol{J}_c^r$) are due to the (inverse) spin Hall effect in the normal metal.

established that the magnitude of the dc spin current density is given by [4]

$$J_s^{SP} = \frac{g_{\uparrow\downarrow}}{2\pi}\frac{1}{2}h\nu P\sin^2\Theta, \tag{1}$$

where ν is the frequency of the microwave, Θ is the cone angle which the precessing magnetization $\boldsymbol{M}$ encloses with the effective magnetic field $\boldsymbol{H}_{eff}$ (the vector sum of the external magnetic field and magnetic anisotropy fields), h is the Planck constant, P is a factor to correct for elliptical precession of $\boldsymbol{M}$ [26] and $g_{\uparrow\downarrow}$ is the spin mixing conductance per unit of interface area and the conductance quantum e^2/h.

As shown in Fig. 1(b), thermal excitations of $\boldsymbol{M}$ also give rise to a spin current. This is the so-called spin Seebeck effect [6,7]. Given a temperature difference ΔT between the electrons in the normal metal and the magnons in the ferromagnet, a dc spin current density [14]

$$J_s^{SSE} = \frac{g_{\uparrow\downarrow}}{2\pi}\frac{\gamma\hbar}{M_s V_a}k_B\Delta T, \tag{2}$$

is generated. We investigate the longitudinal spin Seebeck effect [27], where the temperature gradient is applied across the ferromagnetic-insulator–normal-metal interface. In Eq. (2), $\gamma = g\mu_B/\hbar$ is the gyromagnetic ratio with the effective g-factor g and the Bohr magneton μ_B, M_s is the saturation magnetization and V_a is the magnetic coherence volume given by [14]

$$V_a = \frac{2}{3\zeta(5/2)}\left(\frac{4\pi D}{k_B T}\right)^{3/2}, \tag{3}$$

with the Riemann Zeta function ζ, the spin wave stiffness D and $T = 300$ K for our room temperature experiments.

As depicted in Fig. 1(c), the application of a dc charge current density $\boldsymbol{J}_c$ furthermore allows us to inject a dc spin current density with direction vector $\boldsymbol{J}_s \propto \alpha_{SH}\boldsymbol{J}_c \times \boldsymbol{\sigma}$ into the YIG via the spin Hall effect in Pt [8]. Here, α_{SH} is the spin Hall angle of Pt and $\boldsymbol{\sigma}$ is the spin current polarization. If the magnetization $\boldsymbol{M}$ of the ferromagnet is oriented perpendicular to $\boldsymbol{\sigma}$, $\boldsymbol{J}_s$ can exert a torque on $\boldsymbol{M}$ by being absorbed at the interface. When $\boldsymbol{\sigma}$ is parallel to $\boldsymbol{M}$, the spin current is reflected at the interface, causing a spin current $\boldsymbol{J}_s^r$. Because of the inverse spin Hall effect, $\boldsymbol{J}_s^r$ again generates a charge current density $\boldsymbol{J}_c^r \propto \alpha_{SH}\boldsymbol{J}_s^r \times \boldsymbol{\sigma}$ that effectively changes the electrical resistance of the Pt film.

The net spin current density $J_s^{SMR} = J_s - J_s^r$ for $\boldsymbol{M} \parallel \boldsymbol{J}_c$ is given by [17]

$$J_s^{SMR} = \frac{g_{\uparrow\downarrow}}{2\pi}2e\lambda_{SD}\rho_{Pt}\alpha_{SH}J_c\tanh\frac{t_{Pt}}{2\lambda_{SD}}\eta, \tag{4}$$

where e is the elementary charge, λ_{SD} is the spin diffusion length in Pt, and ρ_{Pt} and t_{Pt} are Pt resistivity and thickness, respectively. We furthermore introduced the correction factor [15,17]

$$\eta = \left[1 + 2g_{\uparrow\downarrow}\rho_{Pt}\lambda_{SD}\frac{e^2}{h}\coth\frac{t_{Pt}}{\lambda_{SD}}\right]^{-1}. \tag{5}$$

As suggested by Eqs. (1), (2), and (4), one should thus observe a scaling $J_s = (g_{\uparrow\downarrow}/2\pi)E$ with an appropriate energy E^{SP}, E^{SSE}, and E^{SMR} that generates the spin pumping, spin Seebeck, and SMR effects, respectively. Note that, due to the inclusion of spin backflow via the correction factor η, the spin mixing conductance enters the linear response expression in a nonlinear fashion by defining an effective excitation energy.

To experimentally test the scaling between J_s and E, we performed a series of spin pumping, spin Seebeck, and spin Hall magnetoresistance measurements on more than 20 samples. Most of these samples consisted of thin film YIG/Pt bilayers with varying Pt thickness. Additionally, we used YIG/X/Pt trilayers in which X was a normal metal (Au or Cu). A complete list of samples, details of their preparation and relevant material parameters can be found in the Supplemental Material [28].

In spin pumping experiments with electrical spin current detection via the inverse spin Hall effect [29,30], it is possible to determine J_s^{SP} from the recorded dc voltage ΔV_{SP} in ferromagnetic resonance (FMR) as [5,11]

$$J_s^{SP} = \frac{\Delta V_{SP}}{C\eta}\frac{1}{L}, \tag{6}$$

with the sample length L and the open-circuit spin Hall conversion efficiency [11]

$$C = \frac{2e}{\hbar}\alpha_{SH}\lambda_{SD}\tanh\left(\frac{t_{Pt}}{2\lambda_{SD}}\right)\frac{\rho_{Pt}}{t_{Pt}}, \tag{7}$$

with $\hbar = h/(2\pi)$. The factor η represents the effect of spin diffusion. Equation (5) is valid for $2\pi\nu\tau_{sf} \ll 1$ with spin flip time $\tau_{sf} \approx 0.01$ ps in Pt [15]. η is therefore a good approximation for our spin pumping data ($2\pi\nu\tau_{sf} \approx 6 \times 10^{-4}$).

A typical experimental V_{SP} trace recorded for a YIG(20 nm)/Pt(7 nm) sample at a fixed microwave frequency $\nu = 9.85$ GHz while sweeping the external magnetic field H is shown together with a schematic of the sample in Fig. 2(a). We observe a resonant Lorentzian line shape of V_{SP} as a function of the external magnetic field [11]. Within experimental error, $V_{SP} = 0$ far away from FMR and ΔV_{SP} is the dc voltage recorded at the resonance magnetic field as indicated in Fig. 2(a). Because YIG is a ferrimagnetic insulator and we took great care to position the sample in a node of the microwave electric field, ΔV_{SP} is not contaminated with rectification voltages [31]. This is supported by the purely symmetric Lorentzian resonance line shapes observed. The sample length L ranged from 3 to 5 mm in the different samples investigated. We determined ρ_{Pt} from four point resistance measurements and t_{Pt} from x-ray reflectometry.

We now turn to the evaluation of $E^{SP} = \frac{1}{2}h\nu P\sin^2\Theta$ [cf. Eq. (1)]. To this end, we extract $\Theta = 2h_{MW}/\Delta H$ [32] from the FWHM line width of the ΔV_{SP} traces, where $\mu_0 h_{MW} = 22$ μT is the circular microwave magnetic field that was determined from paramagnetic resonance calibration. We find $0.08° \le \Theta \le 0.55°$ in the different samples

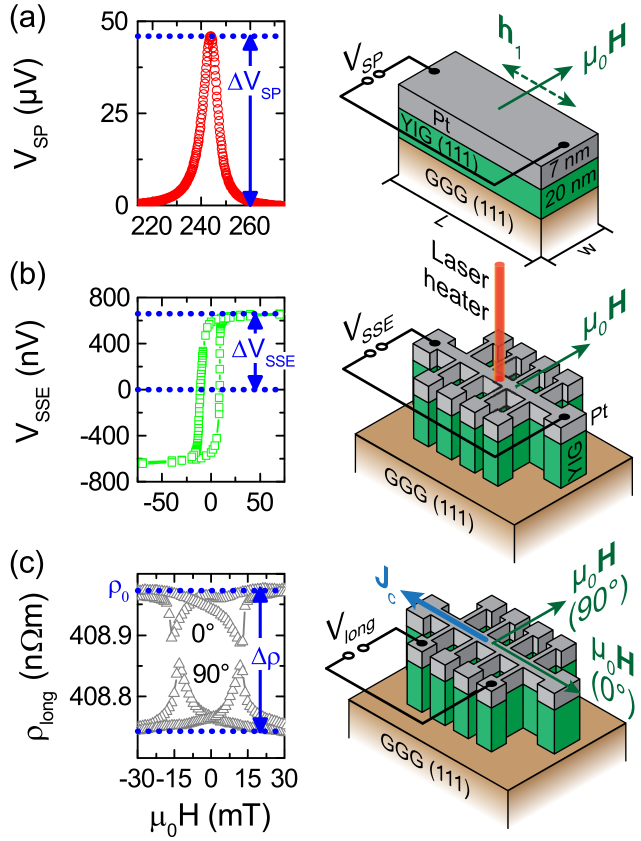

FIG. 2 (color online). (a) Typical spin pumping data obtained from a YIG(20 nm)/Pt(7 nm) bilayer sample as sketched to the right. ΔV_{SP} is extracted at the ferromagnetic resonance as indicated. (b) Data from a spin Seebeck experiment performed using a piece of the same sample. A laser beam is used to generate the thermal perturbation (see text) and ΔV_{SSE} is obtained by taking half of the voltage difference observed between positive and negative saturation magnetic fields in the geometry sketched to the right. (c) dc magnetoresistance measurements are used to extract $\Delta\rho/\rho_0$ as the change in bilayer resistance upon rotating $\boldsymbol{M}$ from parallel (0°) to perpendicular (90°) to $\boldsymbol{J}_{\mathrm{c}}$.

investigated. We calculate the ellipticity correction factor $P = 1.2$ as detailed in Refs. [5,26] using a saturation magnetization $M_{\mathrm{s}} = 140$ kA/m and an effective g-factor $g = 2$ [33]. We are now able to evaluate $J_{\mathrm{s}}^{\mathrm{SP}}$ and E^{SP} as a function of the three parameters $g_{\uparrow\downarrow}$, α_{SH}, and λ_{SD}. We discuss below that with a single set of these parameters we can quantitatively describe the spin pumping, spin Seebeck and SMR data in the context of the spin mixing conductance concept.

In a different set of experiments, using parts of the same samples patterned into Hall bar mesas by optical lithography and subsequent Ar-ion etching, we determined the dc voltage ΔV_{SSE} due to the laser-heating induced spin Seebeck effect [34]. A laser beam of adjustable power ($1.8\ \mathrm{mW} \leq P_{\mathrm{L}} \leq 57\ \mathrm{mW}$) impinges on the main Hall bar (length $L = 950\ \mu\mathrm{m}$ and width $w = 80\ \mu\mathrm{m}$) which is oriented perpendicular to the external, in-plane magnetic field. The laser beam is dominantly absorbed in the Pt layer and yields a temperature difference ΔT between the magnons in YIG and the electrons in the Pt at the YIG/Pt interface. We use a numerical model incorporating a thermal contact resistance between the YIG and the normal metal layers to compute the magnon, phonon, and electron temperature profiles in our samples as a function of layer composition and laser power [35]. We find $0.02\ \mathrm{K} \leq \Delta T \leq 0.9\ \mathrm{K}$. The spin current $J_{\mathrm{s}}^{\mathrm{SSE}}$ is detected via the inverse spin Hall voltage V_{SSE} along the main Hall bar. A typical V_{SSE} curve is shown in Fig. 2(b) as a function of the external magnetic field. The depicted hysteretic V_{SSE} vs H loop is consistent with our previous experiments [34]. The spin current density is extracted from experiment by

$$J_{\mathrm{s}}^{\mathrm{SSE}} = \frac{\Delta V_{\mathrm{SSE}}}{C\eta}\frac{2w}{a^2\pi}, \tag{8}$$

where L from Eq. (6) is now replaced by $a^2\pi/2w$ with the laser spot radius $a = 2.5\ \mu\mathrm{m}$ and the Hall bar width $w = 80\ \mu\mathrm{m}$. This stems from lateral integration over the Gaussian laser spot profile to account for the fact that the sample is heated only locally as demonstrated in Ref. [34] and is valid as long as $a \ll w$, which is the case for all investigated samples. We use the same values for C and η [36] as found for the spin pumping experiments to evaluate $J_{\mathrm{s}}^{\mathrm{SSE}}$. To quantify $E^{\mathrm{SSE}} = \gamma\hbar k_{\mathrm{B}}\Delta T/(M_{\mathrm{s}}V_{\mathrm{a}})$, we use the coherence volume $V_{\mathrm{a}} = (1.3\ \mathrm{nm})^3$ which we obtain from Eq. (3) by using $D = 8.5 \times 10^{-40}\ \mathrm{J\,m^2}$ consistent with theory and a broad range of experiments [37]. The error in the calculated ΔT (and thus E^{SSE}) is dominated by uncertainties in the underlying material parameters [35].

In another set of experiments on the same set of Hall-bar samples we measured the SMR in terms of the change $\Delta\rho$ in bilayer resistance ρ when rotating the magnetization vector in the film plane from $\boldsymbol{M} \parallel \boldsymbol{J}_{\mathrm{c}}$ (ρ_0) to $\boldsymbol{M} \perp \boldsymbol{J}_{\mathrm{c}}$ ($\rho_0 + \Delta\rho$). Typical $\rho(H)$ traces for $\boldsymbol{M} \parallel \boldsymbol{J}_{\mathrm{c}}(0°)$ and $\boldsymbol{M} \perp \boldsymbol{J}_{\mathrm{c}}(90°)$ are shown in Fig. 2(c). We observe the magnetization switching at the coercive magnetic fields that agree with those extracted from our spin Seebeck experiments.

From the SMR data, we extract the spin current density [9,17]

$$J_{\mathrm{s}}^{\mathrm{SMR}} = J_{\mathrm{c}}\frac{\Delta\rho}{\rho_0}\frac{\hbar t_{\mathrm{Pt}}}{\alpha_{\mathrm{SH}}e\lambda_{\mathrm{SD}}\tanh\frac{t_{\mathrm{Pt}}}{2\lambda_{\mathrm{SD}}}} \tag{9}$$

from the experimentally determined $\Delta\rho/\rho_0$. The charge current densities in our experiments were $1.7 \times 10^6\ \mathrm{A/m^2} \leq J_{\mathrm{c}} \leq 1.7 \times 10^9\ \mathrm{A/m^2}$.

We plot $J_{\mathrm{s}}^{\mathrm{SMR}}$ from Eq. (9) as a function of $E^{\mathrm{SMR}} = 2e\lambda_{\mathrm{SD}}\rho_{\mathrm{Pt}}\alpha_{\mathrm{SH}}J_{\mathrm{c}}\tanh[(t_{\mathrm{Pt}}/(2\lambda_{\mathrm{SD}})]\eta$ in Fig. 3(a) (squares) for all samples. In identical fashion, Fig. 3(a) depicts J^{SP} as a function of E^{SP} (circles) and J^{SSE} as a function of E^{SSE} (up triangles). We use a single set of parameters, $g_{\uparrow\downarrow} = 1 \times 10^{19}\ \mathrm{m}^{-2}$, $\alpha_{\mathrm{SH}} = 0.11$ and $\lambda_{\mathrm{SD}} = 1.5$ nm for all samples. These parameters are identical to those extracted from an analysis of the Pt thickness dependence of the SMR [9]. We acquired data points for SMR and spin Seebeck effect on various samples as a function of charge current density or laser power, respectively. We

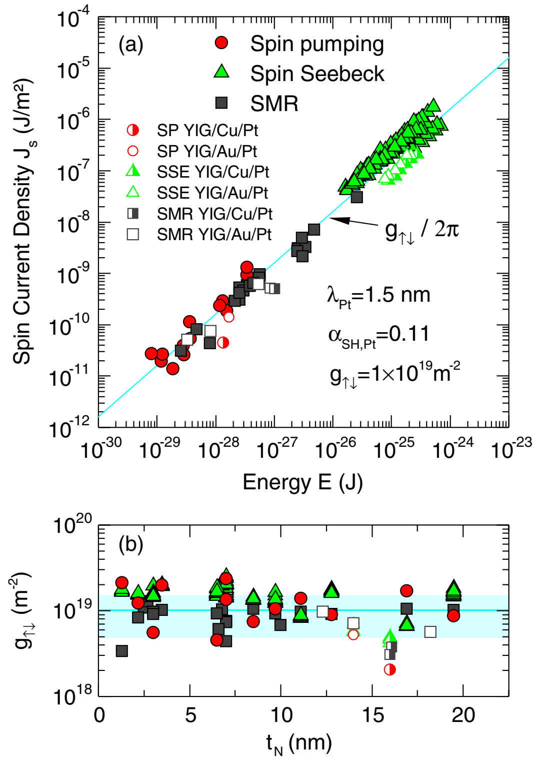

FIG. 3 (color online). (a) Spin current density J_s as a function of the nonequilibrium energy E for all investigated samples as determined in spin pumping (circles), spin Seebeck (triangles), and SMR (squares) measurements. The solid line is the proportionality constant identified in the text as $g_{\uparrow\downarrow}/2\pi$. Open symbols correspond to YIG/Au/Pt trilayer samples and half-filled symbols to YIG/Cu/Pt trilayer samples. (b) The spin mixing conductance as a function of total normal metal thickness [same symbols as in (a)].

furthermore include data recorded using YIG/Au/Pt (open symbols) and YIG/Cu/Pt (half-filled symbols) trilayer samples (symbol shape identifies spin pumping, spin Seebeck or SMR data). To evaluate the trilayer data, we assume vanishing α_{SH} and $\lambda_{SD} \gg t$ for Au and Cu. We thus modify C for spin pumping and spin Seebeck effect as well as J_c and $\Delta\rho/\rho_0$ for the SMR as detailed in the Supplemental Material [28].

Altogether our experimental data span 5 orders of magnitude in J_s and E. In this entire range, we observe that all experimental data points fall on (or close to) one line in the plot. As predicted by theory, the constant of proportionality is found to be $g_{\uparrow\downarrow}/2\pi$. This has several implications. First, and most importantly, Fig. 3(a) is strong evidence for the spin mixing conductance concept, i.e., that spin pumping, spin Seebeck and SMR effects indeed arise from pure spin currents physics. Spurious effects due to static proximity polarization in Pt [21,23,38] can be excluded based on Fig. 3(a), because if the measured spin Seebeck effect and spin Hall magnetoresistance data were caused by anomalous Nernst and anisotropic magnetoresistance effects, a common scaling relation cannot be expected. We observe, however, that the spin mixing conductance is the common scaling factor between spin current density and energy for all data points in Fig. 3(a). This strongly suggests that all three effects have a spin-current based microscopic origin. Our data also enable a quantitative interpretation of the spin Seebeck effect which has remained elusive so far due to the lack of a sufficiently accurate method to quantify the relevant ΔT [35,39]. A spin Hall angle $\alpha_{SH} = 0.11$ and spin diffusion length $\lambda_{SD} = 1.5$ nm work well for our Pt thin films. These parameters agree with the product $\alpha_{SH}\lambda_{SD}$ extracted in previous studies [5,40,41] and more recent findings [9,42–44]. However, their strong correlation prevented an univocal estimate of the separate parameters that were found to vary as $0.004 \leq \alpha_{SH} \leq 0.34$ and $0.5\ \text{nm} \leq \lambda_{SD} \leq 10$ nm for Pt. In our work, owing to the different functional dependence of the three effects on these parameters, we extract λ_{SD} and α_{SH} more reliably.

Figure 3(b) shows $g_{\uparrow\downarrow} = 2\pi J_s/E$ as a function of the total normal metal thickness $t_N = t_{Pt} + t_X$ (X is Au or Cu) for all bilayer and trilayer samples. The symbol definitions are identical to that in Fig. 3(a). The solid line depicts $g_{\uparrow\downarrow} = 1 \times 10^{19}\ \text{m}^{-2}$ and the shaded region corresponds to $0.5 \times 10^{19}\ \text{m}^{-2} \leq g_{\uparrow\downarrow} \leq 1.5 \times 10^{19}\ \text{m}^{-2}$. The majority of our data points lie within the shaded region, so $g_{\uparrow\downarrow}$ is constant within ±50% for all our samples and regardless of the experimental method used to extract it. There is no discernible trend in the J_s to E ratio as a function of Pt (or X/Pt) thickness. This suggests that Eqs. (6), (8), and (9), are sufficiently accurate in the entire thickness range investigated. The unsystematic scatter in $g_{\uparrow\downarrow}$ in Fig. 3(b) can be accounted for as being experimental errors and varying interface properties between the different samples. Our trilayer samples exhibit a $g_{\uparrow\downarrow}$ similar or slightly lower than that of our YIG/Pt bilayers and previous findings for the YIG/Au interface [45,46].

In summary, we have experimentally demonstrated that spin pumping, spin Seebeck, and SMR all share the same purely spintronic origin and thus experimentally validated the spin mixing conductance concept. Spurious contributions due to proximity ferromagnetism in Pt can be ruled out, thereby supporting existing models for SMR and the spin Seebeck effect. A relevant set of parameters for a ferromagnetic-insulator–normal-metal bilayer (or according trilayer) obtained from rather straightforward SMR experiments may be used to predict results for spin Seebeck or spin pumping experiments on the same samples.

Financial support from the DFG via SPP 1538 "Spin Caloric Transport", Project No. GO 944/4-1, the Dutch FOM Foundation, EC Project "Macalo", the National Natural Science Foundation of China (No. 11004036, No. 91121002), Grant-in-Aid for Scientific Research A (Kakenhi) 25247056 and the German Excellence Initiative via the "Nanosystems Initiative Munich"(NIM) is gratefully acknowledged.

*Present address: National Institute of Standards and Technology, Boulder, CO, 80305, USA.
†goennenwein@wmi.badw.de

[1] S. A. Wolf, D. D. Awschalom, R. A. Buhrman, J. M. Daughton, S. von Molnár, M. L. Roukes, A. Y. Chtchelkanova, and D. M. Treger, Science 294, 1488 (2001).
[2] I. Žutić, J. Fabian, and S. Das Sarma, Rev. Mod. Phys. 76, 323 (2004).
[3] G. E. W. Bauer, E. Saitoh, and B. J. van Wees, Nat. Mater. 11, 391 (2012).
[4] Y. Tserkovnyak, A. Brataas, and G. E. W. Bauer, Phys. Rev. Lett. 88, 117601 (2002).
[5] O. Mosendz, V. Vlaminck, J. E. Pearson, F. Y. Fradin, G. E. W. Bauer, S. D. Bader, and A. Hoffmann, Phys. Rev. B 82, 214403 (2010).
[6] K. Uchida, S. Takahashi, K. Harii, J. Ieda, W. Koshibae, K. Ando, S. Maekawa, and E. Saitoh, Nature (London) 455, 778 (2008).
[7] K. Uchida, J. Xiao, H. Adachi, J. Ohe, S. Takahashi, J. Ieda, T. Ota, Y. Kajiwara, H. Umezawa, H. Kawai, G. E. W. Bauer, S. Maekawa, and E. Saitoh, Nat. Mater. 9, 894 (2010).
[8] H. Nakayama, M. Althammer, Y.-T. Chen, K. Uchida, Y. Kajiwara, D. Kikuchi, T. Ohtani, S. Geprägs, M. Opel, S. Takahashi, R. Gross, G. E. W. Bauer, S. T. B. Goennenwein, and E. Saitoh, Phys. Rev. Lett. 110, 206601 (2013).
[9] M. Althammer, S. Meyer, H. Nakayama, M. Schreier, S. Altmannshofer, M. Weiler, H. Huebl, S. Geprägs, M. Opel, R. Gross, D. Meier, C. Klewe, T. Kuschel, J.-M. Schmalhorst, G. Reiss, L. Shen, A. Gupta, Y.-T. Chen, G. E. W. Bauer, E. Saitoh, and S. T. B. Goennenwein, Phys. Rev. B 87, 224401 (2013).
[10] N. Vlietstra, J. Shan, V. Castel, B. J. van Wees, and J. Ben Youssef, Phys. Rev. B 87, 184421 (2013).
[11] F. D. Czeschka, L. Dreher, M. S. Brandt, M. Weiler, M. Althammer, I.-M. Imort, G. Reiss, A. Thomas, W. Schoch, W. Limmer, H. Huebl, R. Gross, and S. T. B. Goennenwein, Phys. Rev. Lett. 107, 046601 (2011).
[12] C. Hahn, G. de Loubens, O. Klein, M. Viret, V. V. Naletov, and J. Ben Youssef, Phys. Rev. B 87, 174417 (2013).
[13] S. M. Rezende, R. L. Rodríguez-Suárez, M. M. Soares, L. H. V.-L. ao, D. L. Domínguez, and A. Azevedo, Appl. Phys. Lett. 102, 012402 (2013).
[14] J. Xiao, G. E. W. Bauer, K. C. Uchida, E. Saitoh, and S. Maekawa, Phys. Rev. B 81, 214418 (2010); J. Xiao, G. E. W. Bauer, K. C. Uchida, E. Saitoh, and S. Maekawa, Phys. Rev. B 82, 099904(E) (2010).
[15] H. J. Jiao and G. E. W. Bauer, Phys. Rev. Lett. 110, 217602 (2013).
[16] H. Adachi, J. I. Ohe, S. Takahashi, and S. Maekawa, Phys. Rev. B 83, 094410 (2011).
[17] Y.-T. Chen, S. Takahashi, H. Nakayama, M. Althammer, S. T. B. Goennenwein, E. Saitoh, and G. E. W. Bauer, Phys. Rev. B 87, 144411 (2013).
[18] K. S. Tikhonov, J. Sinova, and A. M. Finkel'stein, arXiv:1302.0499.
[19] W. Nernst, Ann. Phys. (Berlin) 267, 760 (1887).
[20] T. Miyasato, N. Abe, T. Fujii, A. Asamitsu, S. Onoda, Y. Onose, N. Nagaosa, and Y. Tokura, Phys. Rev. Lett. 99, 086602 (2007).
[21] S. Y. Huang, W. G. Wang, S. F. Lee, J. Kwo, and C. L. Chien, Phys. Rev. Lett. 107, 216604 (2011).
[22] W. Thomson, Proc. R. Soc. London 8, 546 (1856).
[23] S. Y. Huang, X. Fan, D. Qu, Y. P. Chen, W. G. Wang, J. Wu, T. Y. Chen, J. Q. Xiao, and C. L. Chien, Phys. Rev. Lett. 109, 107204 (2012).
[24] Y. M. Lu, J. W. Cai, S. Y. Huang, D. Qu, B. F. Miao, and C. L. Chien, Phys. Rev. B 87, 220409 (2013).
[25] A. Brataas, Y. V. Nazarov, and G. E. W. Bauer, Phys. Rev. Lett. 84, 2481 (2000).
[26] K. Ando, T. Yoshino, and E. Saitoh, Appl. Phys. Lett. 94, 152509 (2009).
[27] K. Uchida, H. Adachi, T. Ota, H. Nakayama, S. Maekawa, and E. Saitoh, Appl. Phys. Lett. 97, 172505 (2010).
[28] See Supplemental Material at http://link.aps.org/supplemental/10.1103/PhysRevLett.111.176601 for a complete list of samples, details of their preparation and relevant material parameters.
[29] J. E. Hirsch, Phys. Rev. Lett. 83, 1834 (1999).
[30] K. Ando, S. Takahashi, J. Ieda, Y. Kajiwara, H. Nakayama, T. Yoshino, K. Harii, Y. Fujikawa, M. Matsuo, S. Maekawa, and E. Saitoh, J. Appl. Phys. 109, 103913 (2011).
[31] L. H. Bai, Y. S. Gui, A. Wirthmann, E. Recksiedler, N. Mecking, C.-M. Hu, Z. H. Chen, and S. C. Shen, Appl. Phys. Lett. 92, 032504 (2008).
[32] Y. Guan, W. Bailey, E. Vescovo, C.-C. Kao, and D. Arena, J. Magn. Magn. Mater. 312, 374 (2007).
[33] P. C. Dorsey, S. E. Bushnell, R. G. Seed, and C. Vittoria, J. Appl. Phys. 74, 1242 (1993).
[34] M. Weiler, M. Althammer, F. D. Czeschka, H. Huebl, M. S. Wagner, M. Opel, I.-M. Imort, G. Reiss, A. Thomas, R. Gross, and S. T. B. Goennenwein, Phys. Rev. Lett. 108, 106602 (2012).
[35] M. Schreier, A. Kamra, M. Weiler, J. Xiao, G. E. W. Bauer, R. Gross, and S. T. B. Goennenwein, Phys. Rev. B 88, 094410 (2013).
[36] We use η from spin pumping theory to approximate spin backflow in the spin Seebeck effect, for which a theory is still being developed.
[37] C. M. Srivastava and R. Aiyar, J. Phys. C 20, 1119 (1987).
[38] D. Qu, S. Y. Huang, J. Hu, R. Wu, and C. L. Chien, Phys. Rev. Lett. 110, 067206 (2013).
[39] M. Agrawal, V. I. Vasyuchka, A. A. Serga, A. D. Karenowska, G. A. Melkov, and B. Hillebrands, Phys. Rev. Lett. 111, 107204 (2013).
[40] T. Kimura, Y. Otani, T. Sato, S. Takahashi, and S. Maekawa, Phys. Rev. Lett. 98, 156601 (2007); T. Kimura, Y. Otani, T. Sato, S. Takahashi, and S. Maekawa, Phys. Rev. Lett. 98, 249901(E) (2007).
[41] L. Vila, T. Kimura, and Y. C. Otani, Phys. Rev. Lett. 99, 226604 (2007).
[42] L. Liu, R. A. Buhrman, and D. C. Ralph, arXiv:1111.3702.
[43] V. Castel, N. Vlietstra, J. B. Youssef, and B. J. van Wees, Appl. Phys. Lett. 101, 132414 (2012).
[44] C. T. Boone, H. T. Nembach, J. M. Shaw, and T. J. Silva, J. Appl. Phys. 113, 153906 (2013).
[45] B. Heinrich, C. Burrowes, E. Montoya, B. Kardasz, E. Girt, Y.-Y. Song, Y. Sun, and M. Wu, Phys. Rev. Lett. 107, 066604 (2011).
[46] C. Burrowes, B. Heinrich, B. Kardasz, E. A. Montoya, E. Girt, Y. Sun, Y.-Y. Song, and M. Wu, Appl. Phys. Lett. 100, 092403 (2012).